Chapter

Single Axis Singularity Mapping for Mixed Skew Angle, Non-Redundant, Single Gimbaled CMG Systems

Eryn A. Culton

Abstract

Control moment gyros are common spacecraft attitude control devices that can be mounted at different orientations within a spacecraft. Some spacecraft need to maximize their maneuverability around a particular axis and, therefore, benefit from particular control moment gyro orientations. This report explains the physics of control moment gyros as attitude control devices and defines a mathematical singularity and its physical manifestation in the spacecraft body. The research continues, analyzing the relation between a control moment gyro's skew angle and its effects on angular momentum magnitude leading to a conclusion defining the best control moment gyro orientations to maximize a spacecraft's yaw maneuverability.

Keywords: rotational mechanics, adaptive control, nonlinear control, control moment gyroscope, momentum exchange, singularity, physics-based control, disturbance decoupling

1. Introduction

Mechanical control has developed over centuries [1–22], expanding original theorems such as Chasle's theorems of motion Phoronomics [23]. With increasing strike capability, advancements in spacecraft technology, and rising political tensions all over the globe, mechanical control has resurfaced as an important research front in order to further current technologies. Opposed nations frequently use satellites on orbit to gather critical intelligence on those around them, a mission that requires precise pointing and an extensive and expansive understanding of the mechanical control envelope provided by the spacecraft's attitude control system. Recent research has been conducted in order to increase the maneuverability of spacecraft with control moment gyroscopes [24–32]. This research takes information and lessons learned from these previous research efforts and builds upon them.

Depending on a spacecraft's mission, it will likely execute a particular kind of attitude maneuver many times during its life span. Characteristic attitude maneuvers should be considered when designing an attitude control system. The type and number of attitude control devices as well as their position within the spacecraft are design choices driven by the physical demands of the attitude maneuvers. These

maneuvers should be considered in order to design an attitude control system that ensures the most angular momentum can be generated around that favored axis while also providing maneuverability in other directions.

Constant-speed, single-gimbaled control moment gyros (CMGs) are common spacecraft attitude control devices that, like reaction wheels, are momentum exchange devices that operate on the law of conservation of momentum in an undisturbed system. Unlike reaction wheels, CMGs do not change their rotational velocity to alter the spacecraft's attitude but, rather, change their direction. Although this ability allows CMGs to uniquely control spacecraft attitude, it also poses challenges: CMGs can only provide torque in a plane orthogonal to their gimbal axis. When a desired torque orthogonal to this plane is commanded, the CMG encounters a mathematical singularity and attitude control is lost.

The locations of these singularities can be plotted 3-dimensionally in order to gain an understanding of the singularity free angular momentum available to command. These singularity maps change based upon the CMG's skew angle within the spacecraft and can be optimized to maximize the singularity free, angular momentum space about a particular axis.

2. Theory

It is necessary to understand how CMGs are commanded and how they physically affect the spacecraft in order to understand how a mathematical singularity causes a spacecraft to lose control. Like any actuator system, a command is entered and a trajectory is generated to reach the commanded position from the initial position; applied to a CMG, a specific rotation is the command and Eq. (1) through Eq. (3) are the equations used to generate the attitude maneuver trajectory [33].

$$\theta = A \sin(\omega t) \tag{1}$$

$$\omega = A\omega \cos(\omega t) \tag{2}$$

$$\dot{\omega} = -A\omega^2 \sin(\omega t) \tag{3}$$

where θ is the gimbal angle, ω is the gimbal rotational velocity, and $\dot{\omega}$ is the gimbal rotational acceleration. To send a command to the CMG actuators, the trajectory is plugged into a feedforward controller that calculates the commanded torque required to set the spacecraft on the created trajectory. The best method of calculating the commanded torque is to use the Newton-Euler equation written in the body frame, represented as Eq. (4).

$$\tau = J\dot{\omega} + \omega \times J\omega \tag{4}$$

The feedforward uses Eq. (5), an adapted version of Eq. (4), to calculate this torque command. Eq. (5) is the nonlinear feedforward control equation based off of the Newton-Euler equation written in the body frame. Since Eq. (5) directly describes the physics of the system, it is the best feedforward control to use.

$$u_{ff} = \hat{J}\dot{\omega}_d + \omega_d \times \hat{J}\omega_d \tag{5}$$

where $\hat{J}$ is the "best guess" spacecraft moment of inertia matrix, $\dot{\omega}_d$ is the desired rotational acceleration, and ω_d is the desired rotation rate. Using this idealized feed forward control eliminates phase lag in the system.

At this point in the system topology, the torque command is converted to a voltage or current and sent directly to the actuators. The actuators move and torque is exerted on the spacecraft as described by Eq. (6).

$$J\dot{\omega} = -J_{CMG}|\dot{\omega}_{CMG}|\hat{\dot{\omega}}_{CMG} \tag{6}$$

where $\dot{\omega}$ is the spacecraft's rotational acceleration, JCMG is the CMG moment of inertia, and $\dot{\omega}_{CMG}$ is the CMG angular acceleration. As the direction of the CMG angular momentum changes, the spacecraft's rotation changes on the other side of Eq. (6). In order to predict how changing the direction of the CMG angular momentum affects the spacecraft, the CMG system orientation must be understood and the angular momentum vectors must be resolved into the three body axes.

For analysis purposes, a simplified, non-redundant, single gimbaled CMG system will be used. This system will consist of three CMG's as pictured in **Figure 1**. To note, the CMG skew angle is defined as the angle between a vertical line parallel to the Z axis at each CMG location and the Z axis; in other words, the gimbal axis would be pointing out from the spacecraft in the x-y plane when $\beta = 0°$ or would be pointing straight up when $\beta = 90°$. In **Figure 1**, β is annotated at its equivalent angle. Also, each angular momentum vector is drawn at its initial position, $\theta = 0°$.

Figure 1 provides a visual aid in generating a set of three equations that resolve the angular momentum of each CMG into the x, y, and z axes. These equations are described in Eqs. (7), (8), and (9).

$$h_x = (\cos\theta_3 - \cos\theta_1 + \sin\beta_2 \sin\theta_2)|H| \tag{7}$$

$$h_y = (\sin\beta_3 \sin\theta_3 - \sin\beta_1 \sin\theta_1 - \cos\theta_2)|H| \tag{8}$$

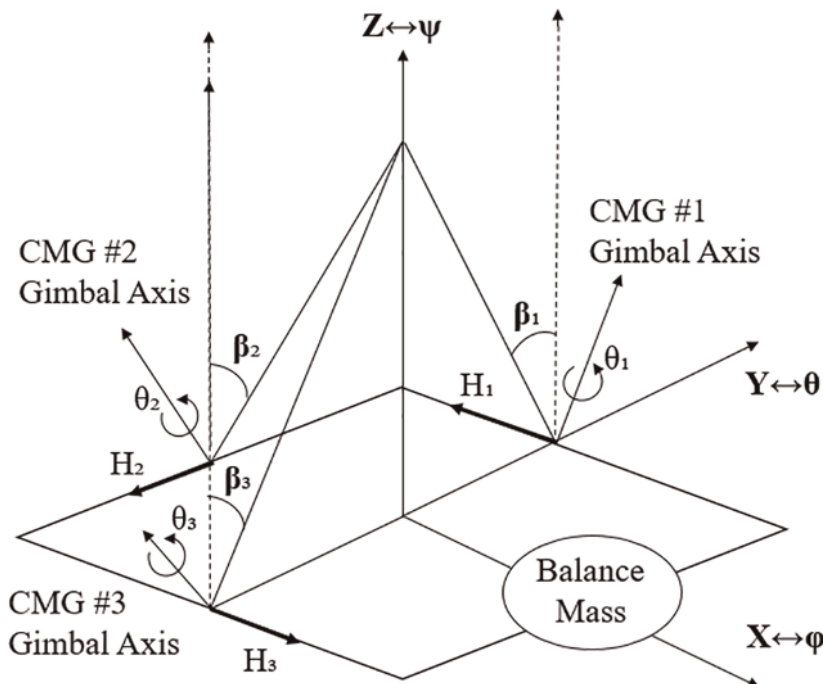$$h_z = (\cos\beta_1 \sin\theta_1 + \cos\beta_2 \sin\theta_2 + \cos\beta_3 \sin\theta_3)|H| \tag{9}$$

Figure 1.
¾ CMG system [34].

where h is angular momentum about a particular axis, β is the skew angle of each CMG, θ is the angle the momentum vector has rotated about the CMG gimbal axis, and H is the maximum angular momentum a single CMG can produce.

The desired torque given from the system described in Eqs. (7), (8), and (9) can be written as Eq. (10), where the desired torque is equal to the partial derivative of angular momentum with respect to the gimbal angle multiplied by the time derivative of the gimbal angle.

$$\tau = \frac{\partial H}{\partial \theta}\frac{d\theta}{dt} \tag{10}$$

The partial derivative of angular momentum with respect to the gimbal angle is found by taking the spatial gradient of Eqs. (7), (8), and (9) which produces a Jacobian matrix, the A matrix. The A matrix describes the components of torque provided by each CMG in each axis; this is represented in Eq. (11).

$$[A] = \frac{\partial \boldsymbol{H}}{\partial \theta_i} = \begin{bmatrix} \sin\theta_1 & \sin\beta_2\cos\theta_2 & -\sin\theta_3 \\ -\sin\beta_1\cos\theta_1 & \sin\theta_2 & \sin\beta_3\cos\theta_3 \\ \cos\beta_1\cos\theta_1 & \cos\beta_2\cos\theta_2 & \cos\beta_3\cos\theta_3 \end{bmatrix} \tag{11}$$

Given the A matrix's definition, Eq. (10) can be written inversely to find the commanded gimbal rotation rates as Eq.(12) where the inverse of A is equal to the reciprocal of the determinant of A multiplied by its cofactor [35].

$$\dot{\boldsymbol{\theta}} = \frac{1}{\det(A)}CoF(A)\boldsymbol{\tau} \tag{12}$$

Eq. (12) encounters a mathematical singularity when the determinant of A equals zero; within the control system, the computer will continually attempt to calculate one over zero and, in the process, send the absurdly large results as torque commands to the CMGs. The CMG actuators follow the randomly large commands and the spacecraft loses attitude control. Physically, this kind of singularity is hit when a particular combination of gimbal angles is reached and the CMG cannot produce torque in the desired direction. These combinations of gimbal angles are defined by the determinant of the A matrix. For the CMG system in **Figure 1** when all skew angles could be different, the determinant of A is evaluated in Eq. (13).

$$\det[A] = \sin\theta_1(\sin\theta_2\cos\beta_3\cos\theta_3 - \sin\beta_3\cos\theta_3\cos\beta_2\cos\theta_2)$$
$$+ \sin\beta_2\cos\theta_2(-\sin\beta_1\cos\theta_1\cos\beta_3\cos\theta_3 - \cos\beta_1\cos\theta_1\sin\beta_3\cos\theta_3) \tag{13}$$
$$- \sin\theta_3(-\sin\beta_1\cos\theta_1\cos\beta_2\cos\theta_2 - \sin\theta_2\cos\beta_1\cos\theta_1)$$

There are a multitude of cases when Eq. (13) is equal to zero, causing a singularity. Within each of these cases, at any chosen combination of skew angles, there are numerous different gimbal angle combinations resulting in a singularity; each of these gimbal and skew angle combinations produces a certain angular momentum in the x, y, and z directions as calculated by Eqs. (7), (8), and (9) respectively. For a particular skew angle combination, there is a gimbal angle combination such that a singularity is hit with the smallest achievable angular momentum: this becomes the maximum angular momentum the entire CMG system can reach before encountering a singularity at that particular skew angle combination set up.
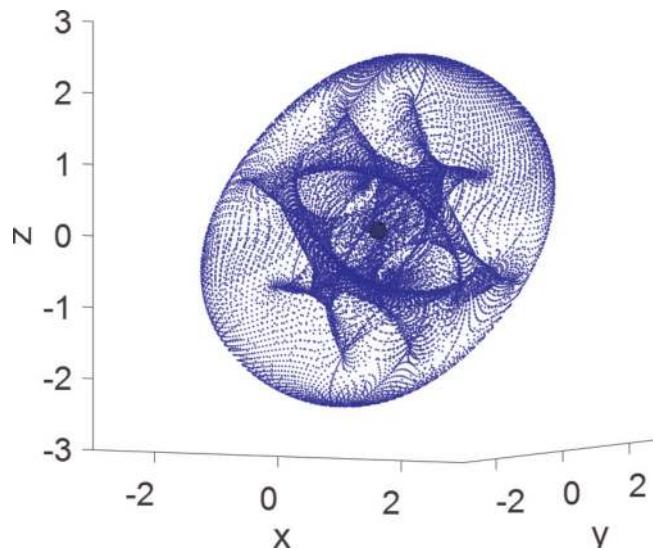
Figure 2.
Restricted angular momentum sphere within entire command space [34].

Although this reduction in the commandable angular momentum has been applied to many spacecraft on orbit, it is extremely limiting. **Figure 2** illustrates this reduction with the black sphere representing the singularity free maximum angular momentum space while the space enclosed with the blue surface represents all valid angular momentum commands. Furthermore, the outer blue surface defines the angular momentum saturation limit for its particular CMG setup. In **Figure 2**, the CMG set up includes three CMGs at equivalent skew angles of 56°.

In an attempt to remove this limit, Sands created a mechanism with which to penetrate this smallest angular momentum and expand the commandable angular momentum to everything up until saturation [32, 36, 37]. This mechanism is called singularity penetration with unit delay (SPUD) [32] and pierces the inner singularity surfaces by sending the CMG actuators valid control commands while the system passes through a singularity. This mechanism is critical in order to reach the maximum angular momentum at a particular axis.

3. Analysis

Defining the maximum angular momentum achievable without encountering a singularity for a CMG system over all possible skew angle combinations can be calculated via two methods: numerically or analytically. To numerically define this surface, the skew angle combinations are discretized and the associated minimum angular momentum is calculated numerically. To analytically define the same surface, each case that makes the determinant of A equal to zero is identified. The equation defining each case is then evaluated for its minimum angular momentum over all gimbal angle combinations for every skew angle. The minimum angular momentum data for all cases is then plotted on a single graph and the minimum angular momentum out of each case is taken as the maximum angular momentum achievable for that skew angle combination.

For this research, numerically calculating the maximum angular momentum without reaching a singularity for each discretized skew angle was chosen over the analytical method because the numeric solution creates a conservative model. The conservative nature of the numeric solution was determined by comparing a

numerically calculated and analytically determined maximum angular momentum plot when all skew angles were equivalent. To compare these methods, however, a discretization size for the numeric solution had to be chosen. Three numeric solutions were plotted with discretizations of 0.1, 1, and 2°. One degree was chosen because using a smaller discretization, such as 0.1°, introduced noise into the plots while using a larger discretization, such as 2°, missed critical data points leading to important singularity locations. The 1° discretization plotted a smooth singularity location line while not skipping any important values. The plots using 0.1 and 2° are pictured in **Figure 3** while the 1° discretization is plotted in **Figure 4** with the analytic solution derived and created in Sands' dissertation [36].

Table 1 describes the mean error and standard deviation between the numerically obtained and analytically obtained data in **Figure 4**.

The numeric results vary from the analytic angular momentum values for most skew angles from 1 to 55° as can be seen in **Figure 4** and **Table 1**. After 55° however, both the numeric and analytic data is equivalent; **Figure 4** shows they plot along the same line while **Table 1** confirms the mean error and standard deviation between the values are both approximately zero. Although the numerically obtained results differ from the analytic values before 55°, the numeric results claim a lower possible
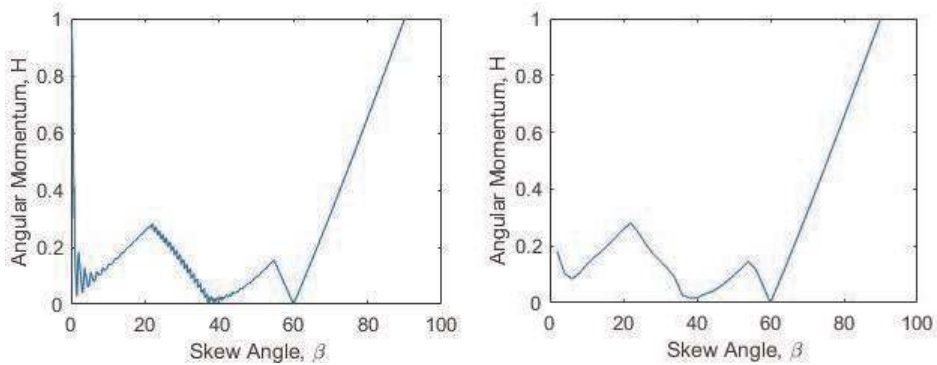

Figure 3.
0.1° discretization (left) versus 2° discretization (right) for numerically determined maximum angular momentum [34].
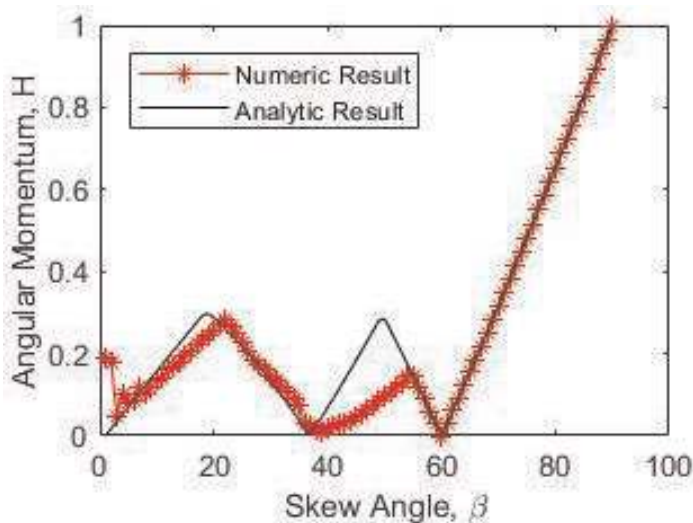

Figure 4.
Numeric versus analytic determination of maximum angular momentum [34].

Data points	μ	σ
1–37	0.0333	0.0388
38–60	0.0811	0.0707
61–90	5.51e-5	1.15e-4
Total	0.0344	0.0530

Table 1.
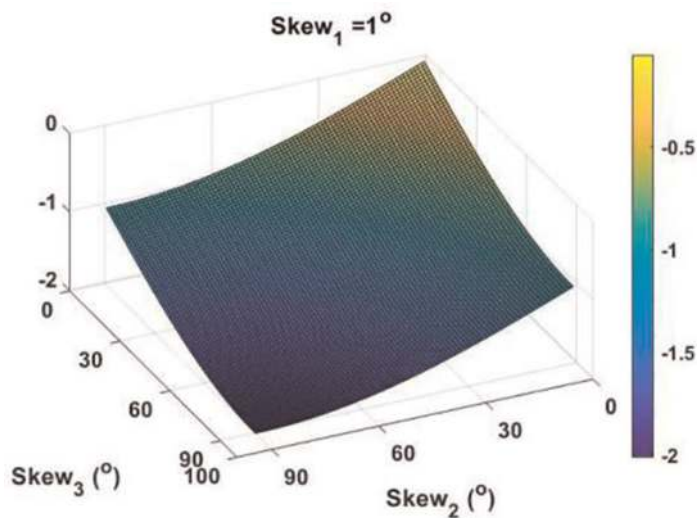*Mean error and standard deviation between numeric and analytic data [34].*

Figure 5.
3-D maximum angular momentum on the z axis for $\beta_1 = 1°$, $\beta_2 = \beta_3 =$ free [34].

angular momentum is possible before reaching a singularity. Using these data points would provide a buffer between where the singularities are expected to be versus where they actually are, protecting the attitude control system from hitting a singularity. Because this buffer is on the "safe" side, the maximum angular momentum without hitting a singularity for a CMG system with different skew angles was determined numerically.

Figure 4 plotted the maximum angular momentum in any direction for a nonredundant CMG system with equivalent skew angles. In order to design an attitude control system for a spacecraft with a characteristic maneuver, a similar figure can be produced plotting only the maximum angular momentum in that favored axis. This research aims to characterize skew angle combination effects on maximum angular momentum around the spacecraft's z axis, in other words, mixed skew angle effects on yaw maneuverability. To analyze this relationship, the maximum achievable angular momentum about the z axis was calculated for different skew angle combinations using the numerical method used to produce **Figure 4**. When creating the plots in **Figures 5** and **6**, the actual angular momentum values were plotted instead of strictly their magnitude; as a result, the plots are negative.

In order to plot the maximum achievable angular momentum about the z axis for all skew angle combinations, a four dimensional plot would be needed. Since this is not achievable, skew angle one was held constant while skew angles two and three were varied from 0 to 90°. Three dimensional plots were created as can be seen in **Figure 5**. However, due to the difficulty of orienting each graph to show the angular momentum magnitude, a color bar was employed instead. This allowed the same data to plot in two dimensions as can be seen in **Figure 6**.
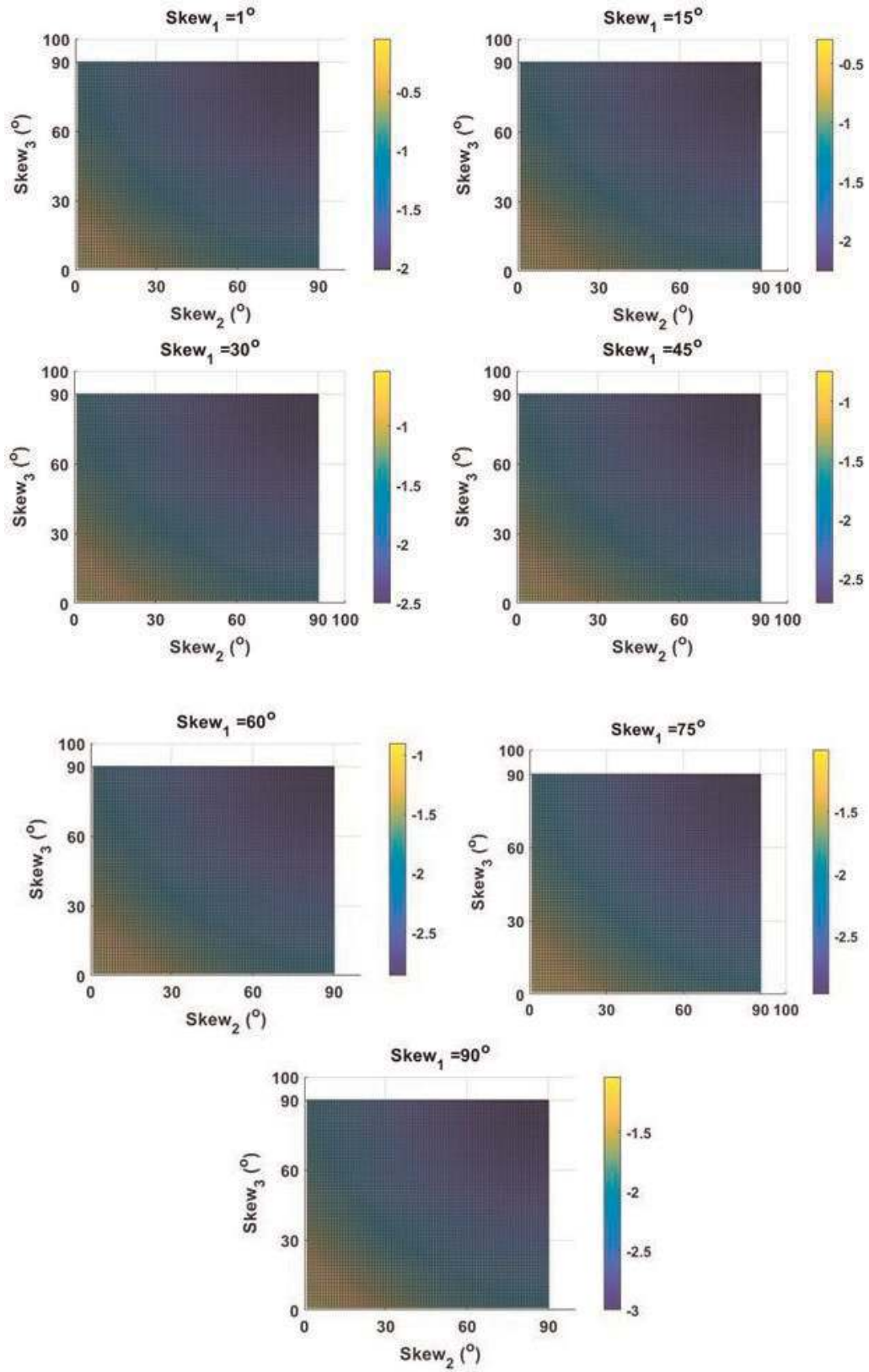
Figure 6.
Maximum angular momentum for $\beta_1 = 1°, 15°, 30°, 45°, 60°, 75°, 90°$, $\beta_2 = \beta_3 = free$ [34].

$|H|$	β_1 (°)	β_2 (°)	β_3 (°)
2.017	1	90	90
2.259	15	90	90
2.5	30	90	90
2.707	45	90	90
2.866	60	90	90
2.966	75	90	90
3	90	90	90

Table 2.
Maximum yaw maneuverability skew angle combinations [34].

Figure 6 illustrates the same trend for all β_1: maximum achievable angular momentum is smallest when both β_2 and β_3 are close to 0° and largest when both β_2 and β_3 are equal to 90°. Additionally, the magnitude of achievable angular momentum increases with β_1. For small β_1, such as 1°, the maximum angular momentum when β_2 and β_3 are close to 0° is 0$|H|$ while for large β_1, such as 90°, the maximum angular momentum when β_2 and β_3 are close to 0° is 1$|H|$. **Table 2** lists the maximum angular momentum and associated skew angles for each plot in **Figure 6**.

Plotting the singularity maps for the skew angle combinations listed in **Table 2** visualizes the commandable angular momentum on the z axis. These mixed skew angle combinations produce the singularity maps pictured in **Figure 7**.

Within **Figure 7**, the highlighted blue surface in each plot contains the singularity defining the maximum achievable angular momentum about the z axis. For skew angle combinations with β_1 lower than 45° and β_2 and β_3 equal to 90°, the saturation limit on the z axis is defined by one of the inner singularity surfaces. For β_1 larger than 45° and β_2 and β_3 equal to 90°, the saturation limit is defined by the outer singularity surface. As long as β_1 is larger than 0°, there are no singularities exactly on the z axis before the saturation limit because there are at least two CMG's capable of exerting maximum angular momentum in the z direction. Since angular momentum can be commanded in that direction regardless of the orientation of the third CMG, there is no singularity until the saturation limit.

4. Conclusion

Drawing from the key points of this research, it is clear that different skew angles create drastically different singularity plots. These singularity plots map out the unattainable torque commands for a particular CMG system, ultimately defining the attitude envelope a spacecraft can achieve within a defined amount of time. As a result of this important relationship, CMG skew angles should be carefully chosen when designing a spacecraft attitude control system.

When designing a non-redundant CMG attitude control system for a spacecraft that needs to maximize its yaw maneuverability, a CMG system with all skew angles equal to 90° would maximize the commandable angular momentum about the z axis as **Figure 6**, **Table 2**, and **Figure 7** all show. The next greatest combination would be to set two of the skew angles equal to 90° and the third skew angle equal to something greater than zero in order to avoid a singularity at the origin.
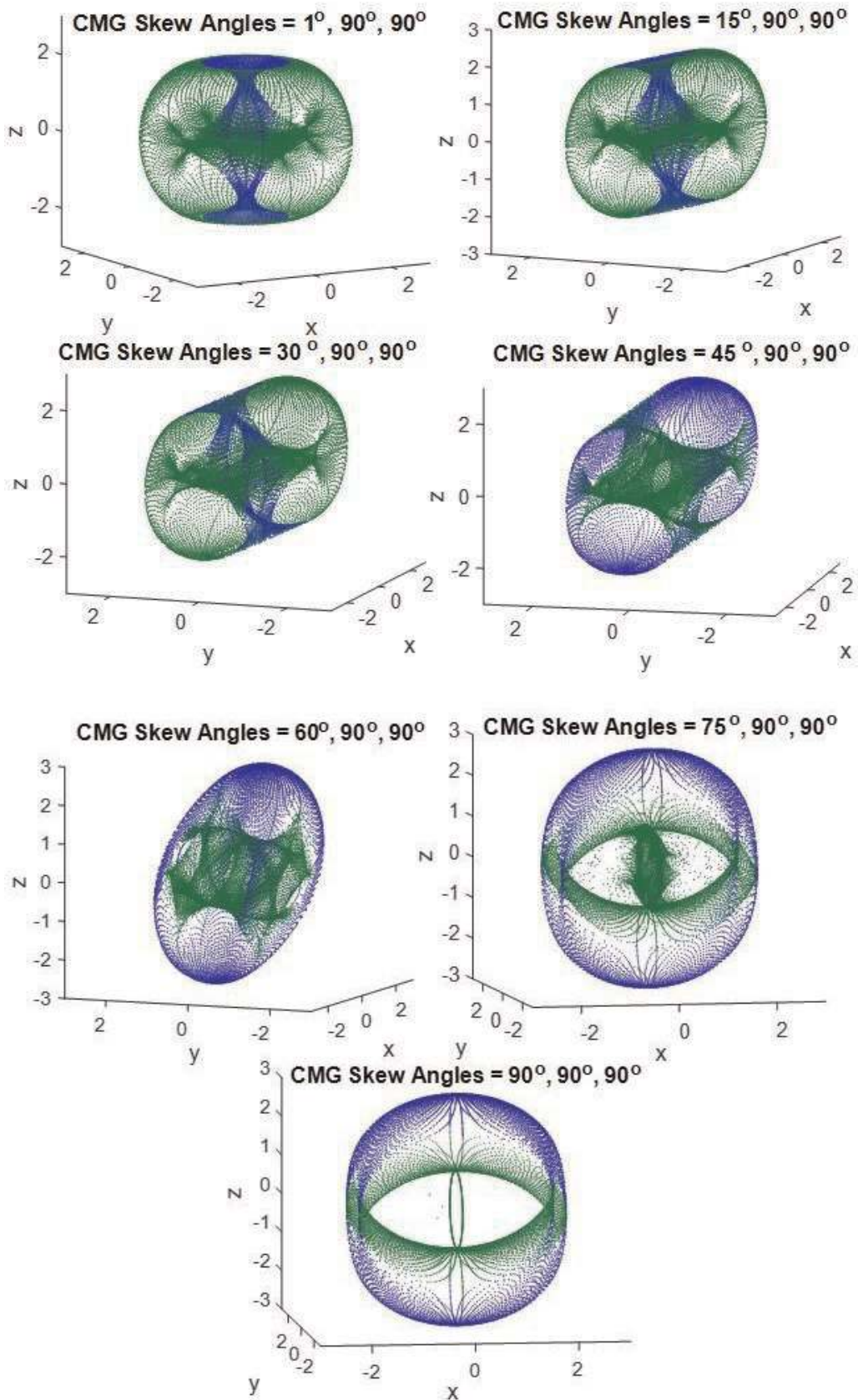
Figure 7.
Singularity maps [34].

Author details

Eryn A. Culton
Naval Postgraduate School, United States Navy, Monterey, CA, USA

*Address all correspondence to: eaculton@nps.edu

IntechOpen

References

[1] Merz J. A History of European Thought in the Nineteenth Century. London: Blackwood; 1903. p. 5

[2] Whittaker E. A Treatise on the Analytical Dynamics of Particles and Rigid Bodies. Cambridge, UK: Cambridge University Press; 1904

[3] Church IP. Mechanics of Engineering. New York: Wiley; 1908. p. 111

[4] Wright T. Elements of Mechanics Including Kinematics, Kinetics, and Statics, with Applications. New York: Nostrand; 1909

[5] Eduard Study (D.H. Delphenich translator), Foundations and goals of analytical kinematics. Sitzber. d. Berl. math. Ges. 1913;**13**:36-60. Available from: http://neo-classical-physics.info/uploads/3/4/3/6/34363841/study-analytical_kinematics.pdf [Accessed: 14 April 2017]

[6] Gray A. A Treatise on Gyrostatics and Rotational Motion. London: MacMillan; 1918 (published 2007 as ISBN 978-1-4212-5592-7)

[7] Rose ME. Elementary Theory of Angular Momentum. New York, NY: John Wiley & Sons; 1957 (published 1995), ISBN 978-0-486-68480-2

[8] Kane T. Analytical Elements of Mechanics Volume 1. New York and London: Academic Press; 1959

[9] Kane T. Analytical Elements of Mechanics Volume 2 Dynamics. New York and London: Academic Press; 1961

[10] Thompson W. Space Dynamics. New York: Wiley and Sons; 1961

[11] Greenwood D. Principles of Dynamics. Englewood Cliffs: Prentice-Hall; 1965 (reprinted in 1988 as 2nd ed.), ISBN: 9780137089741

[12] Fung AC, Zimmermun BG. Digital Simulation of Rotational Kinematics. NASA Technical Report NASA TN D-5302. Washington, DC; 1969. Available from: https://ntrs.nasa.gov/archive/nasa/casi.ntrs.nasa.gov/19690029793.pdf

[13] Henderson DM. Euler angles, quaternions, and transformation matrices—Working relationships. NASA Technical Report NASA-TM-74839. McDonnell Douglas Technical Services Co. Inc.; July 1977. Available from: https://ntrs.nasa.gov/archive/nasa/casi.ntrs.nasa.gov/19770024290.pdf

[14] Henderson DM. Euler angles, quaternions, and transformation matrices for space shuttle analysis. McDonnell Douglas Technical Services Co. Inc., Houston Astronautics Division as NASA Design Note 1.4-8-020, 9 June 1977. Available from: https://ntrs.nasa.gov/archive/nasa/casi.ntrs.nasa.gov/19770019231.pdf

[15] Goldstein H. Classical Mechanics. 2nd ed. Massachusetts: Addison-Wesley; 1981

[16] Kane T, Levinson D. Dynamics: Theory and Application. Boston: McGraw-Hill; 1985

[17] Huges P. Spacecraft Attitude Dynamics. New York: Wiley and Sons; 1986

[18] Wiesel W. Spaceflight Dynamics. 2nd ed. Boston: Irwin McGraw-Hill; 1989. p. 1997

[19] Wie B. Space Vehicle Dynamics and Control. Virginia: AIAA; 1998

[20] Slabaugh GG. Computing Euler angles from a rotation matrix. 1999;**6**(2000):39-63. Available from: http://www.close-range.com/docspacecraftomputing_Euler_angles_from_a_rotation_matrix.pdf

[21] Vallado D. Fundamentals of Astrodynamics and Applications. 2nd ed. El Segundo: Microcosm Press; 2001

[22] Roithmayr C, Hodges D. Dynamics: Theory and Application of Kane's Method. New York: Cambridge; 2016

[23] Chasles M. Note sur les propriétés générales du système de deux corps semblables entr'eux. Bulletin des Sciences Mathématiques, Astronomiques, Physiques et Chemiques (in French). 1830;**14**: 321-326

[24] Sands T, Lu D, Chu J, Cheng B. Developments in angular momentum exchange. International Journal of Aerospace Sciences. 2018;**6**(1):1-7. DOI: 10.5923/j.aerospace.20180601.01

[25] Sands T, Kim J, Agrawal B. 2H singularity free momentum generation with non-redundant control moment gyroscopes. Proc. IEEE CDC; 2006. pp. 1551-1556. DOI: 10.1109/CDC.2006.377310

[26] Sands T. Fine pointing of military spacecraft [dissertation]. Monterey, CA, USA: Naval Postgraduate School; 2007

[27] Kim J, Sands T, Agrawal B. Acquisition, tracking, and pointing technology development for bifocal relay mirror spacecraft. Proceedings of SPIE. 2007. p. 6569. DOI: 10.1117/12.720694

[28] Sands T, Kim J, Agrawal B. Control moment gyroscope singularity reduction via decoupled control. Proc. IEEE SEC. 2009. pp. 1551-1556. DOI: 10.1109/SECON.2009.5174111

[29] Sands T, Kim J, Agrawal B. Nonredundant single-gimbaled control moment gyroscopes. Journal of Guidance, Control, and Dynamics. 2012; **35**:578-587. DOI: 10.2514/1.53538

[30] Sands T, Kim J, Agrawal B. Experiments in control of rotational mechanics. International Journal Automatic Control Intelligent Systems. 2016;**2**:9-22. ISSN: 2381-7534

[31] Agrawal B, Kim J, Sands T. Method and apparatus for singularity avoidance for control moment gyroscope (CMG) systems without using null motion. U.S. Patent 9567112 B1, Feb 14, 2017

[32] Sands T, Kim J, Agrawal B. Singularity penetration with unit delay (SPUD). Mathematics. 2018;**6**:23-38. DOI: 10.3390/math6020023

[33] Baker K, Cooper M, Heidlauf P, Sands T. Autonomous trajectory generation for deterministic artificial intelligence. Electrical and Electronic Engineering. 2018;**8**(3):59-68

[34] Culton E, Sands T. Single axis singularity mapping for mixed skew angle, non-redundant, single gimbaled CMG systems. In: Unpublished manuscript submitted to Advancements in Spacecraft Attitude Control (working title). London, UK: InTech; 2019 Print ISBN: 978-1-78984-802-1. Project in draft form, Due to Publisher April 2019

[35] Sands T, Lu D, Chu J, Cheng B. Developments in angular momentum exchange. International Journal of Aerosol Science. 2018;**6**(1):7

[36] Sands T. Fine pointing of military spacecraft [dissertation]. CA: MAE, NPS; 2010

[37] Agrawal BN, Kim JJ, Sands TA. Method and apparatus for singularity avoidance for control moment gyroscope (CMG) systems without using null motion. US Patent 9,567,112; 2017